11th International Workshop on Ship and Marine Hydrodynamics
Hamburg, Germany, September 22-25, 2019

The Underwater Noise Reduction of Pumpjet Propulsor using Sawtooth Duct with different Inclination Angles

Denghui Qin[1,2], Guang Pan[1,2]*, Yao Shi[1,2], Qiaogao Huang[1,2]

[1] School of Marine Science and Technology, Northwestern Polytechnical University
Xi'an 710072, China
[2] Key Laboratory for Unmanned Underwater Vehicle, Northwestern Polytechnical University
Xi'an 710072, China

*Corresponding author, panguang@nwpu.edu.cn

ABSTRACT

The sawtooth duct noise reduction technology is used for underwater noise reduction of Pumpjet Propulsor (PJP). Flow around the PJP is solved using Detached-Eddy-Simulation (DES) model, while noise is predicted based on Ffowcs-Williams and Hawkings equation. Results show that the sawtooth duct can reduce the sound pressure level of PJP over the frequency range 100-5000 Hz, although it will result in water efficiency loss at low J cases. The sawtooth duct makes the axial velocity distribution of PJP outflow more uniform and reduces the TKE value at the wake region of PJP. The maximum water efficiency is reduced about 2% by sawtooth duct, and the open water efficiency at low J case gradually decreases with the increase of the sawtooth inclination angle. Significantly, the sawtooth duct reduce the overall sound pressure level about 3.82-7.17 dB, while causes the efficiency loss about 1.67%-2.56% at the design point. The sawtooth duct with sawtooth inclination angle 10° has the most great noise reduction about 7.17 dB with only 1.93% openwater efficiency loss at the design point of PJP.

Keywords: Pumpjet Propulsor; The underwater noise reduction technology; The sawtooth duct; The inclination angle

1 INTRODUCTION

Over the past few decades, the ambient noise in the sea has increased by 12 dB, due to the significant increase of number and size for commercial shipping vessels in the world [1]. In order to ensure sustainable shipping, the underwater radiated noise (URN) from commercial shipping has been targeted by environmentalists [2]. International Maritime Organization (IMO) and Marine Environmental Protection Committee (MEPC) [3, 4] have made calls and initiated activities to study the URN from commercial shipping to help in the development of potential regulations. The underwater noise of vessels mainly including: 1. Machinery noise, 2. Propeller noise, 3. Hydrodynamic noise. Furthermore, the propeller noise usually dominates the overall noise spectrum [5]. Therefore, noise predictions for propellers have always been an important issue in naval architecture.

Pumpjet propulsor (PJP) is a new type of underwater propeller. At present, the researches of PJP are mainly focused on the experiment and numerical simulation. The experiment of an underwater vehicle equipped with a PJP is carried out by Ch. Suryanarayana et al [6]. Stefan Ivanell [7] simulated the hydrodynamic performance of a torpedo with PJP using computational fluid dynamics method (CFD). Pan Guang et al [8] studied the hydrodynamics of an underwater vehicle equipped with PJP. Lin Lu et al [9] predicted the hydrodynamic performance of a PJP based on the Reynolds Averaged Navier Stokes (RANS) CFD method. Qin et al [10] discussed the influence of tip clearances on PJP hydrodynamic performance based on CFD method. As for the underwater radiated noise of PJP, there are very little publications, and

most papers are about the noise research of the single propeller. So the noise prediction of pumpjet propulsor and its noise characters still need more research.

The flight of most owl species is so quiet and not audible to their prey. The noise reduction mechanisms for the special morphological features of owl wing have already been tested for their applicability on technical airfoils, resulting in sawtooth trailing edge technology [11]. Subsequently, the sawtooth trailing edge technology was applied to the aero-engine exhaust nozzle, called chevron exhaust nozzles, which is proved to be effective in reducing jet noise and is widely used in the aviation industry. GE [12] developed the chevron nozzle for jet noise reduction for high bypass ratio separate flow exhaust systems. It is found that the sawtooth trailing edge technology can achieve the 2-3 EPN (Effective Perceived Noise) dB noise reduction. This makes the sawtooth trailing edge technology getting more and more attention. Callender [13] carried the far-field noise test of Chevron nozzles in the University of Cincinnati Nozzle Acoustic Test Facility (UCNATF). The spectral and directivity results show that the overall sound pressure level (SPL) is reduced in ranging from 3 to 6 dB. The sawtooth trailing edge noise reduction technology is world widely used in the aviation field, but to authors' best knowledge, it has not been used in the noise reduction for underwater propeller. However, in view of the similar geometry and flow between the pumpjet propeller and the aircraft engine jet nozzle, it is worth exploring whether the sawtooth trailing edge can change the turbulent structure of the PJP in the wake region and whether it can produce the same noise reduction effect on the PJP.

2 METHODOLOGY

The governing equations of incompressible fluid flow are Reynolds Averaged Navier-Stokes (RANS) equations that can be written as the continuity equation and momentum conservations as follows:

$$\frac{\partial u_i}{\partial x_i} = 0 \tag{1}$$

$$\frac{\partial (u_i)}{\partial t} + \frac{\partial (u_i u_j)}{\partial x_j} + \frac{\partial p}{\partial x_i} - \frac{\partial \tau_{ij}}{\partial x_j} = 0 \tag{2}$$

where ρ is the fluid density, x_i and x_j (i = 1, 2, 3, j =1, 2, 3) are the Cartesian coordinate components, respectively. u_i are the components of the absolute velocity in the inertial system, p is the pressure, $\tau_{ij} = \nu_T(\partial u_i / \partial x_j + \partial u_j / \partial x_i)$ is the stress tensor, and $\nu_T = 1/Re + \nu_t$, with ν_t being the turbulent viscosity calculated by means of a proper turbulence model (described later) and Re being the Reynolds number.

Firstly, the steady flow of propeller will be simulated based on the RANS with Shear-Stress-Transport (SST) $k-\omega$ model [14-15]. Secondly, the DES simulation of PJP is carried out and then time dependent pressure data is used as the input to the FW-H equation to predict the underwater radiated noise of PJP. In this paper, the DES method based on the Spalart & Allmaras model [16]was used. Due to the limitation of the length of the article, the specific equation is no longer introduced.

Finally, the noise is predicted based on FWH equation, which is shown as follow:

$$\frac{1}{a_0^2}\frac{\partial^2}{\partial t^2} - \nabla^2 p' = \frac{\partial^2}{\partial x_i \partial x_j}\left\{T_{ij} H(f)\right\} + \frac{\partial}{\partial t}\left\{\left[\rho_0 v_n + \rho(u_n - v_n)\right]\delta(f)\right\} - \frac{\partial}{\partial x_i}\left\{\left[P_{ij} n_j + \rho u_j (u_n - v_n)\right]\delta(f)\right\} \tag{6}$$

Where a_0 is the sound velocity in the far field and T_{ij} is the Lighthill tensor defined as follows:

$$T_{ij} = \rho u_i u_j + P_{ij} - a_0{}^2(\rho - \rho_0)\delta_{ij} \tag{7}$$

And P_{ij} is the compressive stress tensor. u_n is the flow velocity normal to the surface (f=0) and v_n is the surface velocity component normal to the surfaces. $\delta(f)$ is the Dirac delta function and $H(f)$ is the

Heaviside function. p' is the far-field sound pressure ($p' = p - p_0$). n_j is the unit normal vector indicating the exterior region. u_i and u_j is the flow velocity in the i and j axis direction.

3 VALIDATION

3.1 Flow simulation methodology validation

In this paper, numerical verification is carried out with a worldwide employed propeller (the DTRC4119 propeller), which was presented by 20th ITTC (International Towing Tank Conference) Propulsor Committee [17]. The geometry data of the propeller is presented in Tables 1. And the computational domain and boundary conditions is shown in Fig. 1. The computational domain is a cylinder with 6D diameter, extending from -3D to 7D in the streamwise direction. Structural mesh is used here. Specifically, the first boundary layer height around the blades is 0.005 mm which ensures the y^+ values of walls are less than 1, and the growth rate is 1.05. The detail of the blades mesh is illustrated in zoomed-in view in Fig.1. In addition, with the aim of noise prediction, a rotating domain with 1.25D diameter and 4D length is created around the propeller whose axis coincides with the propeller rotation axis. The mesh of this domain is refined to capture the evolution of wake vortices, and the outer surface is selected as the acoustic source. The total number of grids is about 8 million.

Table 1: Parameters of the DTRC4119 propeller

Parameters	Propeller diameter (mm)	Number of blades	Hub-Diameter ratio	Direction of rotation	Expanded blade area ratio
Value	304.8	3	0.2	Right hand	0.608

The advance ratio J is defined as $J = U_\infty / (nD_h)$, where U_∞ denotes the free stream velocity, n is the blade rotating velocity and the D_h is the diameter of propeller. ρ_f is the density of fluid. The thrust coefficient $K_T = Thrust / (\rho_f n^2 D_h{}^4)$ and torque coefficient $K_Q = Torque / (\rho_f n^2 D_h{}^5)$ are defined, respectively. The relative percentage errors ΔK_T and ΔK_Q are defined as shown below.

$$\Delta K_T(\%) = \frac{K_{TCFD} - K_{TEXP}}{K_{TEXP}} * 100 \tag{9}$$

$$\Delta K_Q(\%) = \frac{K_{QCFD} - K_{QEXP}}{K_{QEXP}} * 100 \tag{10}$$

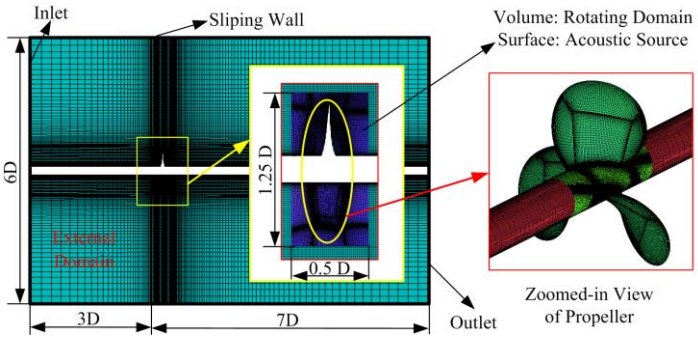

Figure 1: Computational domain and boundary conditions for DTRC4119 propeller.

In the RANS simulation of DTRC 4119, the SST $k-\omega$ turbulence model is applied. The inlet is set as velocity inlet boundary U_∞=1.6m/s and the outlet is set as pressure outlet boundary type with an average relative static pressure 0 Pa. The rotating speed is changed according to different work conditions. And the

contacting surface between the rotating and static domain is set as the interface to enable the exchange of information between the two sub domains. In addition, the SIMPLEC algorithm is used for the pressure-velocity coupling. The pressure and momentum terms are discretized by two order upwind scheme.

S.D.Jessup [18] presented detailed measurement for flow around propeller DTRC 4119. So the numerical simulation results of hydrodynamic coefficient are compared with the experimental data in Table 2. Based on the results, all the relative errors of the thrust and torque coefficient are always less than 2% with maximum relative error ΔK_T=1.65% at J=0.7. So the numerical simulation results have a good agreement with the experimental data. Consequently, it is indicated that the numerical simulation method with the SST $k-\omega$ turbulence model is applicable and reliable for the numerical simulation of propeller steady flows.

Table 2: Parameters of the DTRC4119 propeller

J	$K_{T\,CFD}$	$K_{T\,EXP}$	ΔK_T	$10\,K_{QCFD}$	$10\,K_{QEXP}$	ΔK_Q
0.7	0.2033	0.2000	1.65%	0.3618	0.3600	0.50%
0.833	0.1477	0.1460	1.16%	0.2817	0.2800	0.61%
0.9	0.1189	0.1200	-0.92%	0.2401	0.2390	0.46%

3.2 Noise prediction methodology validation

After conducting steady state calculation, the DES simulation is carried out for acoustic prediction based on the FW-H equation with the initial value of steady flow. The outer surface of rotating domain around propeller is defined as the noise source surface. Solution for acoustic prediction of DTRC 4119 propeller operated at 120 RPM with a forward velocity of 1.6 m/s is carried out. Central difference scheme is used for time discretization and the time iteration step is set as $0.0014s$. Density and velocity of sound in the undisturbed medium for standard medium are 1026 kg/m3 and 1500 m/s, respectively. The reference pressure for Sound Pressure Level calculations is $P_{ref}=1\mu Pa$.

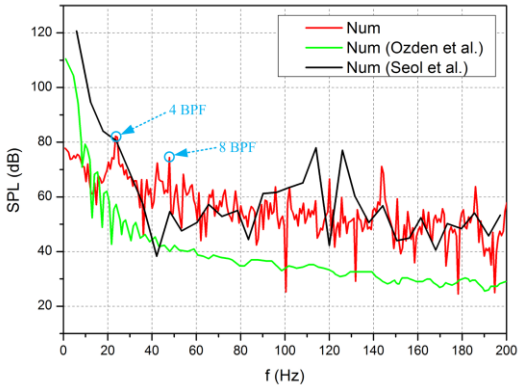

Figure 2: Comparison of noise predictions for DTRC4119 propeller with results by Seol et al. [19] and Ozden et al. [20].

Due to that there is no noise experimental data of DTRC 4119, the noise numerical simulation results in this paper are compared with the other peoples' numerical results. The receiver is located 10R from the propeller center and 0° angle from the inlet flow direction. The sound pressure level at the receiver (see Fig. 2) is predicted. As shown, the numerical simulation value of sound pressure level for DTRC4119 propeller is similar with the result of Seol et al [19], and a little bigger than Ozden et al [20]. It is understandable that Ozden et al predict the noise using a URANS solver with SST $k-\omega$ model and the noise sample steps is also only 720. The noise numerical results show (red line as showed in Fig. 2) that the sound pressure level spectrum for propeller consists of the discrete spectrum and broadband spectrum. The discrete spectrum is located at Blade Passing Frequency (BPF) and its multiples, which can be clearly observed as peaks at the harmonics of BPF. Basically speaking, the trends and values of the spectrum curve are similar to those numerical results of others.

4 NUMERICAL SET-UP

4.1 Test case

The geometry 3D model of PJP is shown in Fig. 3 (a), with 11 rotor blades, 9 stator blades. The rotors rotate clockwise (seen from front). The diameter of PJP is D =0.26 m and the length of duct is L =0.4 m. In order to make the next analysis more concise, the two different models are defined as normal pumpjet propulsor model (NPM) and the sawtooth duct pumpjet propulsor model (SDPM) respectively. The rotor blades and stator blades geometries are all the same in both models.

The model of pumpjet propulsor with sawtooth duct is shown as Fig. 3 (b). The size of sawtooth duct is shown in Fig. 4. D_1 is the diameter of NPM outlet disc, and D_2 is the diameter of SDPM outlet disc. The length of sawtooth is L_s =0.025 m and the angel of sawtooth is $\beta = 70^\circ$. The tooth number of the sawtooth duct is N=18. Sawtooth inclination angle is defined as α, shown in Fig. 4. In order to study the performance of SDPM models with different sawtooth size, four different SDPM models are created as shown in Fig. 5. The difference of those models is the value of α. The four models are called SDPM0; SDPM1; SDPM2 and SDPM3, with α=0°; 5°;10° and 15° respectively.

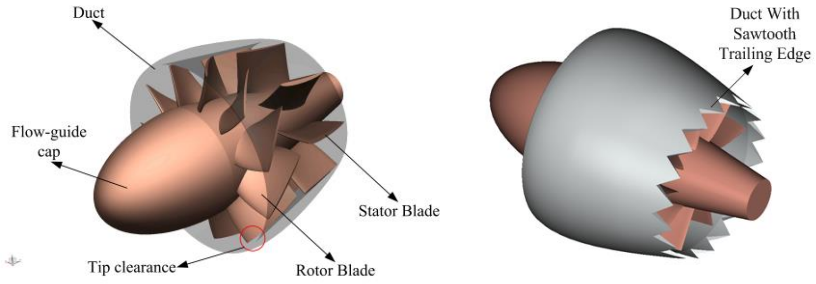

(a) The normal pumpjet propulsor model (NPM). **(b)** The sawtooth duct pumpjet propulsor model (SDPM0).

Figure 3: The pumpjet propulsor geometry 3D models.

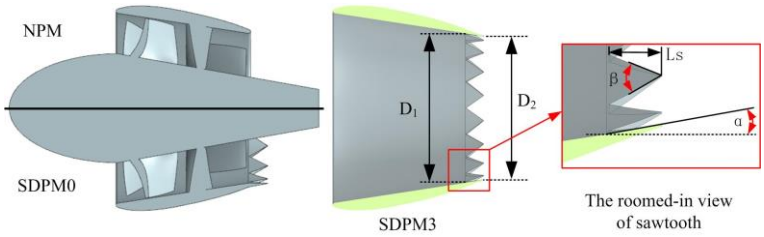

Figure 4: The size of sawtooth duct.

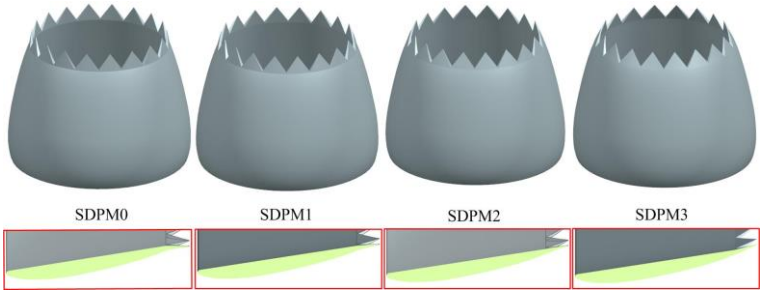

Figure 5: The different sawtooth duct models.

4.2 Mesh and Boundary condition

The computational domain and boundary conditions are shown in Fig. 6. The computational domain is a cylinder with a diameter 5D, and extends 3L upstream and 7L downstream from the origin O, respectively. The computational domain consisted of the rotor domain, stator domain, the noise domain and external domain. In order to predict noise, a domain around the propeller called “noise domain” is created. The noise

domain is a cylinder with 1.5D diameter and 4D length and the outer wall of this domain is selected as the noise source.

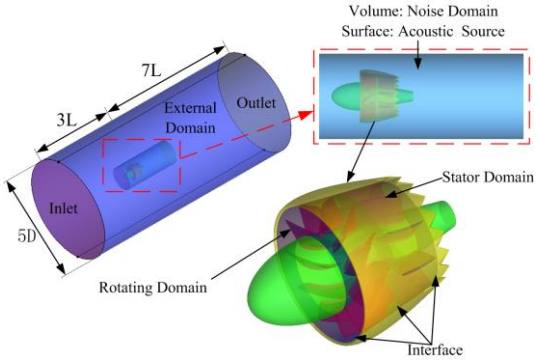

Figure 6: The different sawtooth duct models.

The structured grids are used in this research. Fig. 7 shows the meshes of blades and duct for NPM and SDPM3. For all the models, the meshes of blades are same, and the only difference is the mesh of duct and hub. To satisfy the requirements of the DES algorithm, the y^+ value of the walls is restricted to $y^+ \approx 10$. The total number of grids for NPM is approximately $12,000,000$, while the number of cells for the other four SDPM models corresponds to $14,000,000$.

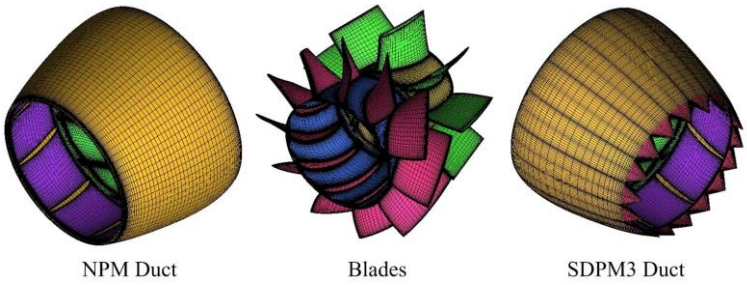

Figure 7: The mesh details of the blades and duct for NPM and SDPM3.

The inlet boundary is set as normal speed, V=25.72 m/s, while the rotational speed is 2600-3800 revolutions per minute (RPM). The turbulence intensity is 5% as the default. The averaged static pressure of outlet is set as 10 MPa. The flow of PJP is solved by ANSYS FLUENT (Version 15, ANSYS Inc.) based on finite volume method solver. In the DES simulation, The SIMPLEC algorithm is adopted and the convection and diffusion terms are discretized by using the 2nd order upwind scheme. Specifically, the time term is discretized by using the bounded 2nd order implicit time discretization. The time step setting satisfy that Courant-FriedrichsLewy (CFL) <1.

5 RESULTS DISCUSSION

5.1 The effects of the sawtooth duct on the open water performance of PJP

The flow simulations of NPM and SDPM models with inlet velocity $V = 25.72\ m{\cdot}s^{-1}$ and rotational speeds (N) varying from 2600 to 3800 RPM are carried out. Fig. 8 shows the thrust and torque coefficients and open water efficiency results for NPM.

As showed, the thrust and torque coefficients of the rotor and stator-duct system all decrease linearly with the increase of the advance coefficient J. Also torque coefficients of the rotor, K_{M_t}, is almost the same as the torque coefficients of stator and duct system K_{M_s}, which shows that this propulsor is well designed and has a good torque performance.

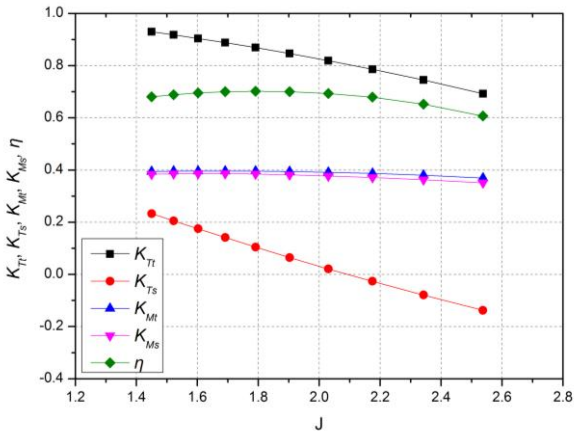

Figure 8: Thrust and torque coefficients and open water efficiency curves of NPM

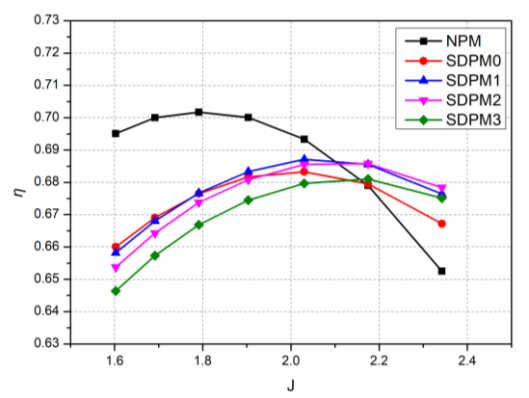

Figure 9: The open water efficiency curves of NPM and SDPM models.

In order to explore the effects of sawtooth duct with different inclination angles on the open water performance of PJP, the open water efficiency results of NPM and SDPM0-SDPM3 models are compared in Fig. 9. As shown, the open water efficiency curves of SDPM models show the same change law with that of NPM. However, the open water efficiencies of SDPM models are smaller than NPM at J<2.03; but bigger than that at J>2.18. What's more, the open water efficiency of NPM reaches its maximum 70.17% at J=1.79, but SDPM0 has a peak about 68.33% at J=2.03, and SDPM3 has a peak about 68.18% at J=2.18. Hence, it means that the maximum water efficiency has reduced about 2% by sawtooth duct. And the maximum operating point moves to from low J to high J direction. The sawtooth duct caused the efficiency loss at low J case but improve the open water efficiency at high J case. Furthermore, at most cases, the open water efficiency decreases slowly from SDPM0 to SDPM3. The open water efficiency at low J case decreases with the increase of the sawtooth inclination angle α.

5.2 The effects of sawtooth duct on the flow of PJP

To analysis the effects of sawtooth duct on the flow of PJP, the steady RANS flow results of NPM and SDPM models are contrasted in the case J=1.90, which is the design point of PJP. The 3D streamlines around the normal duct and SDPM0 are illustrated in Fig. 10 (a) and (b), respectively. As showed, for NPM, the flow in the outer of duct is sucked to inner. As for SDPM, due to the pressure difference of side surfaces and top-bottom surfaces, the flow is sucked into the sawtooth channel from the surface of duct and a pair of vortexes is generated in every sawtooth channel. There appear two low velocity zones near the root in every sawtooth channel for SDPM (see Fig. 10 (b)), in contrast to a circular low velocity zone behind the trailing edge of duct for NPM. Therefore, there is a pair of counter rotating vortexes in every sawtooth channel, and the two vortexes formed in the root of sawtooth and develop following two side sawtooth surfaces along the streamwise direction.

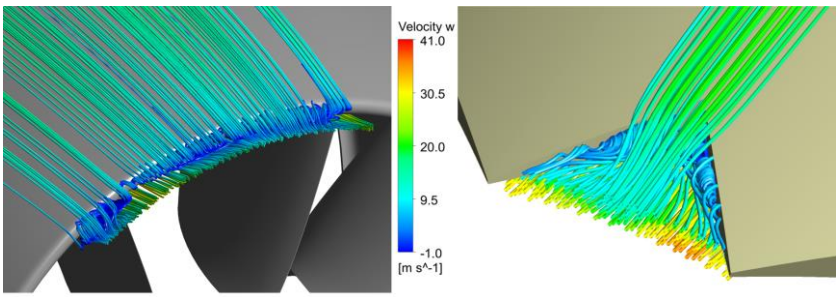

(a) NPM. (b) SDPM0.

Figure 10: The 3D streamlines around duct which colour is defined by axis velocity for NPM and SDPM0.

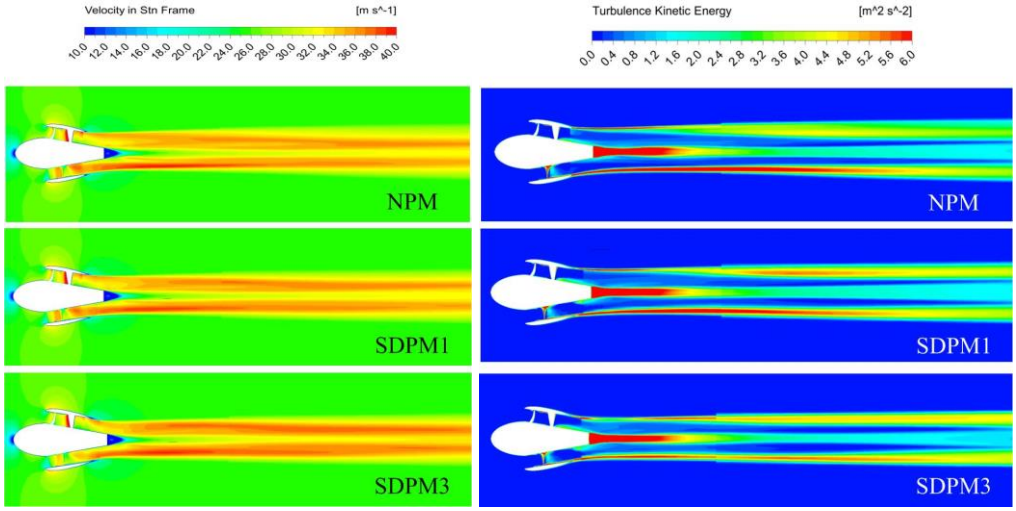

(a) velocity contours. (b) TKE contours.

Figure 11: The overview axis velocity contours and TKE contours of center plane for NPM and SDPM models.

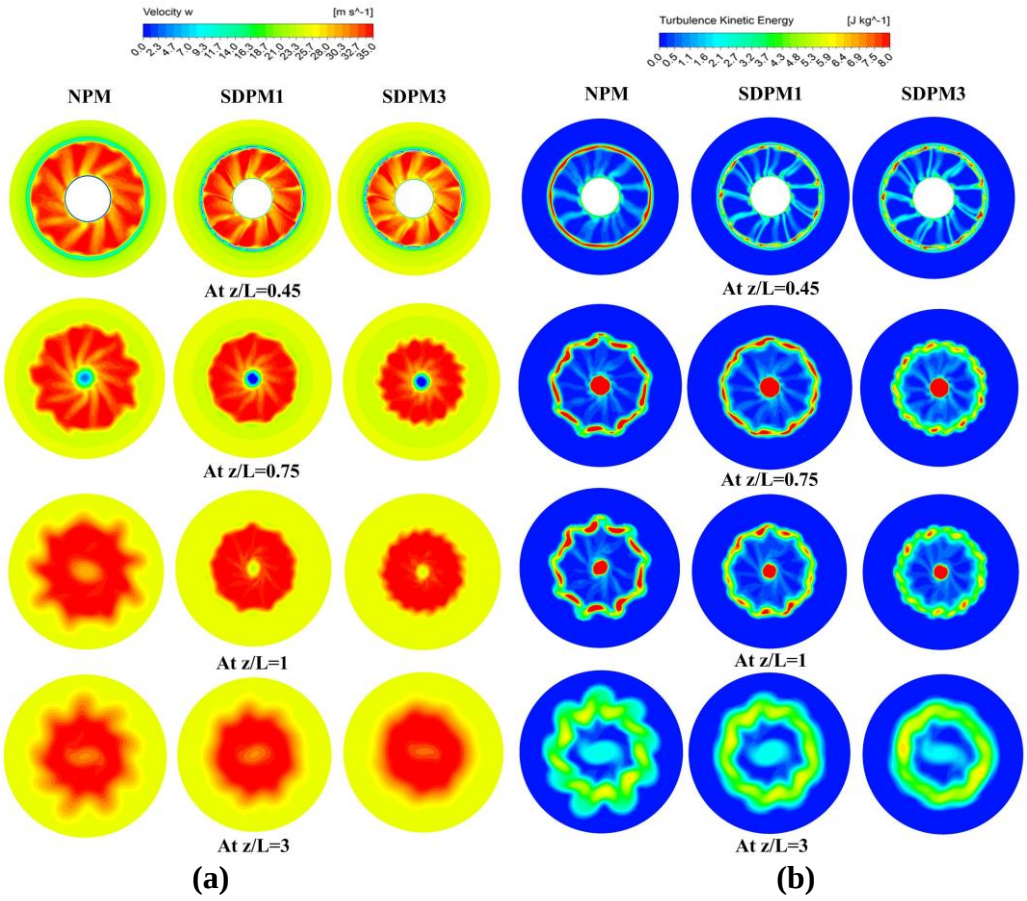

Figure 12: The axis velocity and TKE contours at different z locations for NPM and SDPM models.

To study the effect of sawtooth on the flow wake region of PJP, the velocity and turbulence kinetic energy (TKE) of NPM and SDPM models are discussed. Fig. 11 has visualized the velocity magnitude and the TKE contours of center plane for NPM and SDPM models. As shown in the Fig. 11 (a), the axis velocity in the wake region of SDPM is nearly same with that of NPM. For SDM3, the outflow of PJP is slightly high than that of NPM and SDPM1 due to that the diameter of outlet disc for SDPM3 is smaller than that of NPM and SDPM1. The sawtooth has obviously changed the flow in the wake region behind the duct.

Furthermore, the axis velocity contours at different z locations (z/L=0.45; 0.75; 1; 3) for NPM, SDPM1 and SDPM3 are compared in Fig. 12 (a). Firstly, at z/L=0.45; there appearing low velocity zones in every sawtooth channel whose number is 18 due to the sawtooth vortexes discussed before. Then, from z/L=0.75 to z/L=3, the high velocity zones in the wake region of NPM, SDPM1 and SDPM3 show a big difference. The outer boundary of high velocity propulsor outflow (the red area) is clearly change by sawtooth duct. For SDPM3, the outer boundary of red area shows a petal shape with sawtooth number N=18 (see the figure at z/L=0.75), while for NPM, the shape of outer boundary for high velocity propulsor outflow is changing from nearly round to petal shape which number is 9, which means the stator blade channel flows began to dominate the outflow. By contrast the contours at z/L=3, we can see that the shape of outflow outer boundary is nearly always maintain as uniform circles for SDPM3. From SDPM1 to SDPM3, the axis velocity distribution of PJP wake region is more and more uniform. The pair of counter rotating vortexes in every sawtooth channel is similar as fluid mixer and the vortexes strongly exchange the fluid of high velocity outflow with the surrounding fluid. The bigger sawtooth inclination angle α, the more fully flow mixing caused by the sawtooth, and the more uniform axis velocity distribution in the wake region.

Moreover, the high TKE area in the wake region of SDPM3 is obviously less than that of NPM (see Fig. 11 (b)), which means that the sawtooth duct significantly reduced the TKE in the most wake region. The more detail information of the TKE reducing is shown in Fig. 12. (b). Based on the results, the SDPM3 shows a great TKE reduction than SDPM1 compared with that of NPM. It is easy to understand that the pair of counter rotating vortexes in every sawtooth channel helps the mixing of the propulsor outflow with surrounding flow and so prompted the dissipation of TKE in the wake region.

5.3 The effects of sawtooth duct on the noise of PJP

The underwater radiated noises of PJP are predicted. The noise sampling time step is $5\times10^{-5}s$. And 10000 time steps CFD results are sampled. The sound pressure level is corrected to 1 m (in dB and $P_{ref}=1\mu Pa$). The noise receiver is located behind the PJP, 1m far away from the PJP center point.

Fig. 13 has visualized the sound pressure level (SPL) results of receiver locations of NPM compared to SDPM models in the case J=1.9 (N=3200 rpm). In this case, the rotor blade passage frequency (BPF) is $f_{BPF}=586.67Hz$. The noise frequency spectrums of PJP models are mainly composed by two parts: the discrete tonal noise and the broadband noise. Several peaks are illustrated in Fig. 13 (b). For NPM, the first obvious peak is located at about $f=160Hz$, which is exactly as much as 3 times of hub rotating frequency. The high peak at about $f=585Hz$ (at about 1 BPF) can also be observed.

A comparison of the SPL curve of both models indicates that the noise of SDPM has the same noise spectrum characteristic as NPM. Based on the results, the SPL of SDPM0 is similar with the SPL of NPM, but the SPL values of SDPM1, 2 and 3 are obviously smaller than the value of NPM. In low frequency 10-100 Hz, the noise reduction of SDPM models are not so good or even improve the noise value compared with NPM, for example SDPM1. But generally speaking, the SPL values at frequency range 100-5000 Hz are reduced by sawtooth duct, which shows the sawtooth duct has a good noise reduction.

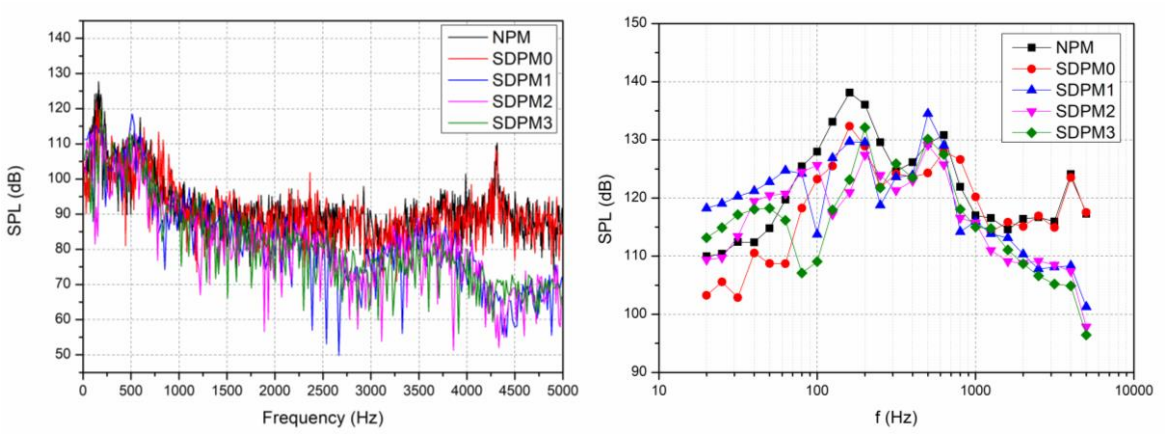

(a) 1 Hz frequency band (b) 1/3 octave band

Figure 13: Underwater noise predictions of NPM and SDPM models (in 1 Hz frequency band) in the case J=1.90.

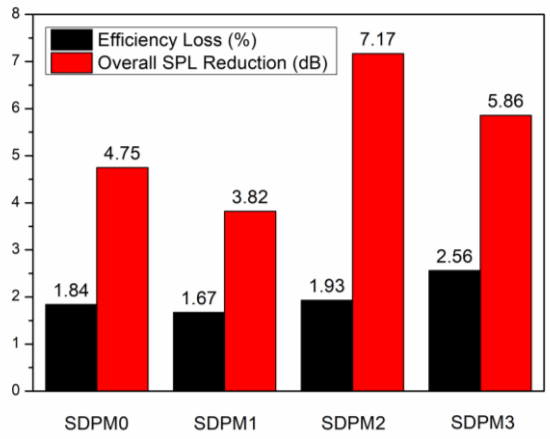

Figure 14: The efficiency loss and overall SPL reduction of SDPM models at J=1.90.

In addition, the efficiency loss values and overall sound pressure level (OASPL) results for SDPM models at the case J=1.90 are shown in Fig. 14. As shown, the SDPM models have an OASPL reduction about 3.82-7.17 dB, while caused the efficiency loss about 1.67%-2.56%. Consequently, the sawtooth has reduced the noise level of PJP at almost the frequency range 100-5000 Hz. The noise spectrum characteristic of SDPM models is similar with that of NPM, but reduced in the amplitude. The SDPM2 shows the most great noise reduction about 7.17 dB with only 1.93% efficiency loss.

6 CONCLUSION

In this study, the sawtooth duct noise reduction technology is used for underwater noise reduction of pumpjet propulsor (PJP). A normal pumpjet propulsor model (NPM) and four sawtooth duct pumpjet propulsor models (SDPM) have been presented to study the effect of the sawtooth duct on the hydrodynamic and noise preference of PJP. Numerical simulations were carried out to analysis the effect of the sawtooth duct on the hydrodynamic, flow field, and noise of PJP. The underwater radiated noise prediction of PJP is carried based on the DES simulation and FW-H equations.

The numerical results reveal that:

1) The maximum water efficiency has reduced about 2% by sawtooth duct. The sawtooth duct caused the efficiency loss at low J case but improve the open water efficiency at high J case. The open water efficiency at low J case decreases with the increase of the sawtooth inclination angle α.

2) There is a pair of counter rotating vortexes in every sawtooth channel, formed in the root of sawtooth and develop following two side sawtooth surfaces along the streamwise direction. The pair of vortexes prompts the dissipation of TKE in the wake region. The sawtooth duct makes the axial velocity distribution of PJP outflow more uniform and reduces the TKE value at the wake region of PJP.

3) The SDPM models have reduced the noise level of PJP at almost the frequency range 100-5000 Hz, and have an OASPL reduction about 3.82-7.17 dB, while caused the efficiency loss about 1.67%-2.56%. The SDPM2 shows the most great noise reduction about 7.17 dB with only 1.93% efficiency loss.

ACKNOWLEDGEMENTS

This work was supported by the National Natural Science Foundation of China (Grant No.51479170; No.51709229).

REFERENCES

[1] Hildebrand, J. A. (2009). Anthropogenic and natural sources of ambient noise in the ocean. *Marine Ecology Progress Series*, 395, 5-20.

[2] Aktas, B., Atlar, M., Turkmen, S., Shi, W., Sampson, R., Korkut, E., & Fitzsimmons, P. (2016). Propeller cavitation noise investigations of a research vessel using medium size cavitation tunnel tests and full-scale trials. Ocean Engineering, 120, 122-135.

[3] IMO, (2011). Noise from commerical shipping and its adverse impact on marine life- development of an international standard for measurement of underwater noise radiated from merchant ships. MEPC 62nd session Agenda item 19. MEPC 62/19.

[4] MEPC, 2009. Noise From Commercial Shipping and Its Adverse Impacts on Marine Life. MEPC 60/18 18 December 2009.

[5] Ross, D. (2013). Mechanics of underwater noise. Elsevier.

[6] Suryanarayana Ch， Satyanarayana B， Ramji K， et al(2010). Experimental evaluation of pumpjet propulsor for an axisymmetric body in wind tunnel. International Journal of Naval Architechture and Ocean Engineering， 2：24-33.

[7] Ivanell S. (2001) Hydrodynamic simulation of a torpedo with pump jet propulsion system. Stockholm：Royal Institute of Technology.

[8] Pan, G., Hu, B., Wang, P., Yang, Z., and Wang, Y. (2013), “Numerical Simulation of Steady Hydrodynamic Performance of a Pump-jet Propulsor,” Journal of Shanghai Jiao Tong University, Vol. 47, 932-937.

[9] Lu, L., Pan, G., & Sahoo, P. K. (2016). CFD prediction and simulation of a pumpjet propulsor. International Journal of Naval Architecture and Ocean Engineering, 8(1), 110-116.

[10] Qin, D., Pan, G., Huang, Q., Zhang, Z., & Ke, J. (2018). Numerical Investigation of Different Tip Clearances Effect on the Hydrodynamic Performance of Pumpjet Propulsor. International Journal of Computational Methods, 15(05), 1850037.

[11] Howe, M. S. (1991). Noise produced by a sawtooth trailing edge. The Journal of the Acoustical Society of America, 90(1), 482-487.

[12] Martens, S. (2002). Jet noise reduction technology development at GE aircraft engines. ICAS Paper, 842.

[13] Callender, B., Gutmark, E. J., & Martens, S. (2005). Far-field acoustic investigation into chevron nozzle mechanisms and trends. AIAA journal, 43(1), 87-95.

[14] F. R. Menter, Two-equation eddy-viscosity turbulence models for engineering applications, Aiaa Journal 32 (8) (1994) 1598-1605.

[15] P. Huang, J. Bardina, T. Coakley, Turbulence modeling validation, testing, and development, NASA Technical Memorandum 110446

[16] Spalart, P., & Allmaras, S. (1992, January). A one-equation turbulence model for aerodynamic flows. In 30th aerospace sciences meeting and exhibit (p. 439).

[17] K. Koyama, Comparative calculations of propellers by surface panel method-workshop organized by 20th ittc propulsor committee, Ship Research Institute, Supplement (15).

[18] S. D. Jessup, An experimental investigation of viscour aspects of propeller blade flow, The Catholic University of America, Dissertation for Ph. D.

[19] H. Seol, B. Jung, J.-C. Suh, S. Lee, Prediction of non-cavitating underwater propeller noise, Journal of Sound and Vibration 257 (1) (2002) 131-156.

[20] M. Ozden, G. Avci, E. Korkut, A numerical study on prediction of noise characteristics generated by a propeller, in: 10th International Conference on Hydrodynamics-ICHD2012, St. Petersburg, Russia, 2012.